Detailed study of the S $2p^{-1} \rightarrow X\,^1A_1(2b_1^{-2})$ normal Auger spectra of H_2S

M. Poygin,[1] R. Püttner,[1] M. Martins,[1,*] V. Pennanen,[2] M. Jurvansuu,[2] Y. H. Jiang,[1] H. Aksela,[2] S. Aksela,[2] and G. Kaindl[1]
[1]*Institut für Experimentalphysik, Freie Universität Berlin, Arnimallee 14, D-14195 Berlin-Dahlem, Germany*
[2]*University of Oulu, Department of Physical Sciences, P.O. Box 3000, 90401 Oulu, Finland*
(Received 26 April 2006; published 13 July 2006)

High-resolution S $2p^{-1}$ photoelectron spectra and S $2p^{-1} \rightarrow X\,^1A_1(2b_1^{-2})$ normal Auger electron spectra (AES) of H_2S were measured for various photon energies in the range from 180 to 240 eV. The equilibrium geometry, vibrational energies $\hbar\omega$, and anharmonicities $x\hbar\omega$, for the S $2p^{-1}$ intermediate and $X\,^1A_1(2b_1^{-2})$ final states were derived from the energy splittings and the intensity distributions of the vibrational substates. The relative intensities of the various S $2p^{-1} \rightarrow X\,^1A_1(2b_1^{-2})$ normal Auger transitions as well as the lifetimes of the various S $2p^{-1}$ core-ionized states were also derived. In addition to the S $2p^{-1} \rightarrow X\,^1A_1(2b_1^{-2})$ transitions, some weak structures were observed in the AES, with intensities that exhibit pronounced photon-energy dependences.

DOI: 10.1103/PhysRevA.74.012711 PACS number(s): 33.80.Eh, 33.20.Tp, 33.15.Dj

I. INTRODUCTION

In molecules, two-hole final states created by an Auger decay subsequent to core ionization are normally dissociative leading to broad spectral features. However, in some special cases, when both holes are created in nonbonding orbitals, the two-hole final state can be stable or quasistable with respect to dissociation. This has been shown for HCl or DCl [1–3], HBr or DBr [4,5], and HI [6]. Intermolecular forces are, however, very sensitive to any changes in the valence shell and transitions to these undissociative states will therefore lead to large changes in the equilibrium geometry and to extended vibrational fine structure. In the present paper we address the S $2p^{-1} \rightarrow X\,^1A_1(2b_1^{-2})$ normal Auger transitions in H_2S. This is the only normal Auger transition in this molecule, which displays narrow peaks with vibrational fine structure, since the molecular orbital $2b_1$ is the only one directed out of the molecular plane, with the consequence that it is nonbonding, i.e., the $2b_1^{-2}$ final state is stable with respect to dissociation. Any other combination of two holes in the final state leads to dissociation. Thus, the S $2p^{-1} \rightarrow X\,^1A_1(2b_1^{-2})$ normal Auger transition in H_2S has been widely studied. In 1991 Svensson *et al.* reported on medium-resolution normal Auger electron spectra (AES) of H_2S [7]. In those spectra, the ligand-field splitting of the S $2p_{3/2}^{-1}$ level into the components $4e_{1/2}$ and $5e_{1/2}$ could not be resolved. As a result of this unresolved splitting, in combination with a strong suppression of the S $2p_{3/2}^{-1}4e_{1/2} \rightarrow X\,^1A_1(2b_1^{-2})$ transition that was not known in those days, the first photoelectron spectra (PES) and AES resulted in different spin-orbit splittings of the S $2p$ level. Only three years later, spectra with improved resolution revealed the strong suppression of the S $2p_{3/2}^{-1}4e_{1/2} \rightarrow X\,^1A_1(2b_1^{-2})$ transition resolving the discrepancy [8]. The most recent work [9] presented a detailed analysis of high-resolution AES focusing on the intensity of the different S $2p^{-1} \rightarrow X\,^1A_1(2b_1^{-2})$ Auger transitions, the vibrational progression, and the core-hole lifetimes of the various S $2p$ levels. In this work, we continue with the studies of the S $2p^{-1} \rightarrow X\,^1A_1(2b_1^{-2})$ normal Auger transitions in H_2S and derive the equilibrium geometry of H_2S in intermediate and final states by detailed fit analyses of the AES and PES.

As mentioned above, the core-ionized intermediate state S $2p^{-1}$ in H_2S is split threefold by spin-orbit and ligand-field splitting into the sublevels $3e_{1/2}$, $4e_{1/2}$, and $5e_{1/2}$. The energy splitting of the S $2p_{3/2}^{-1}$ level caused by molecular field and vibrational splitting is comparable to the lifetime broadening of the core hole. This causes an overlap of the various intermediate states, resulting in lifetime interference contributions in the Auger spectra, i.e., the ionization and the Auger decay have to be described as one-step processes.

We recently performed a detailed analysis of the Br $3d^{-1} \rightarrow 4p\pi^{-2}$ normal Auger spectra of HBr and DBr taking spin-orbit and ligand-field splittings as well as vibrational fine structure into account [5]. This led to a reassignment of the spectrum and to a deeper insight into the potential energy surfaces of the states involved. We also considered the vibrational lifetime interference contribution originating from a one-step process and showed that this effect has a much stronger influence on the spectrum than hitherto believed—although higher vibrational substates are very weak in the PES that probe the intermediate core-hole state. Subsequently, we improved our data analysis so that we were able to take electronic lifetime interference into account in a semiempirical way, and applied this procedure to the Cl $2p^{-1} \rightarrow 3p\pi^{-2}$ normal Auger transition of HCl and DCl [3]. In these studies it has been found that electronic lifetime interference terms play only a minor role in the spectrum. This is due to the large number of final states since for a full description of the final state, the symmetry of the photoelectron and the Auger electron have to be taken into account.

The present work provides an analysis of the S $2p^{-1} \rightarrow X\,^1A_1(2b_1^{-2})$ normal Auger spectra of H_2S similar to the one published recently for HBr and DBr [4] as well as for HCl and DCl [3]. In the present case, the normal AES and PES were fitted simultaneously, and electronic lifetime interference terms were taken into account in a semiempirical way. We report on consistent values for the equilibrium

*Present address: Institut für Experimentalphysik, Universität Hamburg, Luruper Chaussee 149, D-22761 Hamburg, Germany.

distances, vibrational energies, and anharmonicities of the potential-energy curves of the $2b_1^{-2}$ final states as well as on relative Auger rates for all S $2p^{-1} \rightarrow 2b_1^{-2}$ transitions. It had been shown for HBr that such detailed understanding of the normal AES can be extremely helpful for the analysis of resonant AES [10].

We use the following notation for describing the electronic levels: The five core levels are mainly atomiclike and sulphur derived, and we use S $1s$, S $2s$, S $2p_{1/2}$, and S $2p_{3/2}$ as notations. The ligand field leads to three S $2p$ levels that are labeled in the order of decreasing binding energy as $3e_{1/2}$, $4e_{1/2}$, and $5e_{1/2}$. The valence orbitals are strongly influenced by the symmetry of the molecule, and we employ the symmetry notation with $4a_1$, $2b_2$, $5a_1$, and $2b_1$ for the four occupied valence orbitals.

II. EXPERIMENTAL SETUP

The PES and AES of H_2S were recorded at the gas-phase beamline I411 of the 1.5-GeV electron storage ring Max II in Lund, Sweden. The measurements were performed with photon energies between 180 and 240 eV. The PES were taken with a photon energy resolution of about 15 meV [full width at half maximum (FWHM)], using a 10-μm exit slit for the monochromator. The AES were recorded at a lower photon energy resolution (of $\approx$0.6 eV), in order to increase the count rate; this is possible since the photon resolution of the excitation process does not contribute to the total resolution of an AES. The beamline endstation is equipped with a high-resolution Scienta SES-200 hemispherical electron analyzer that can be rotated in the plane perpendicular to the incoming beam. All spectra were collected at the magic angle of 54.7° and by retarding the electrons entering the analyzer to a pass energy of 10 eV. This corresponds to a kinetic-energy resolution of about 20 meV. The spectra were calibrated to the energy values given in Refs. [8,9]. The H_2S gas used in the measurements was purchased from Sigma-Aldrich Chemie GmbH, with a purity of 99.9% that was checked by recording the photoelectron spectra in the valence region in order to detect possible impurities, such as water.

III. DATA ANALYSIS

The data analysis has been described in detail in a previous publication [5]. Here we summarize only the major ideas and describe the differences from the previous procedure [5]. The AES and PES were fitted simultaneously using the same set of parameters when possible. This allowed us to describe the two spectra with $\simeq$30 fit parameters, leading to more reliable fit results for the common parameters. In the fit procedure, the molecular field and spin-orbit splitting were taken into account, as well as post-collision interaction (PCI) and vibrational fine structure.

Since the energy splittings between the S $2p_{3/2}^{-1}4e_{1/2}$ and S $2p_{3/2}^{-1}5e_{1/2}$ intermediate states and the vibrational substates of the different S $2p^{-1}$ core-ionized states are of the same order of magnitude as the lifetime width Γ, the process cannot be described in a two-step model. Consequently, the excitation and deexcitation processes were described in a one-step model according to the Kramers-Heisenberg formula [11] taking lifetime interferences into account.

The relative intensities of transitions to the various vibrational sublevels are proportional to the squares of the Franck-Condon factors (FCFs), which are determined by the overlap between the vibrational wave functions in the potential energy surfaces in the ground, the intermediate, and the final states. To calculate the FCF, Morse potentials for the ground state, the intermediate S $2p^{-1}$ core-ionized state, and the $2b_1^{-2}$ final state were assumed; possible differences in the potential energy surfaces of the various ligand field components of the $2p^{-1}$ core-ionized state were neglected. A Morse potential is defined by three parameters: the vibrational energy $\hbar\omega$, the anharmonicity $x\hbar\omega$, and the equilibrium distance along the corresponding normal coordinate Q. Based on these three parameters for each Morse potential, the FCF for an electronic transition can be calculated with an algorithm based on the work of Halman and Laulich [12] as well as Ory *et al.* [13]. The values for the potential energy surface of the ground state were taken from the literature [14]. The three parameters for the Morse potentials of the S $2p^{-1}$ intermediate and the $2b_1^{-2}$ final state were varied in each iteration step during the fit analysis in order to improve the consistency with the experimental results.

The calculations of the vibrational matrix elements for the fit analysis were not performed in real space but in the space of the normal coordinates, resulting in changes of the normal coordinates upon electronic transition ΔQ. Polyatomic molecules possess more than one normal coordinate, and the various normal coordinates Q_i can normally not be associated with a single bond distance r_i or a single bond angle γ_i. In order to convert the changes of the normal coordinates to changes of the geometrical parameters of the molecule, such as intermolecular distances and angles, it is necessary to know the relationship between normal coordinates and internal coordinates, which—in the case of H_2S—are two H-S distances r_1 and r_2 and the H-S-H bonding angle γ. This relationship can be established from first principles, i.e., from the Lagrange equations for a three-body system, using an algorithm described in Ref. [15]. In the basis set of the internal coordinates, the force matrix $\mathbf{F}$ is diagonal in good approximation. The matrix elements of the matrix $\mathbf{F}$, i.e., the force constants, were taken from Refs. [16–18]. The nondiagonal elements turn out to be small and were neglected in the present calculation. The gravity matrix in internal coordinates $\mathbf{G}^{-1}$ can be derived from the usual mass matrix $\mathbf{M}$ using $\mathbf{G}^{-1}=\mathbf{B}'\mathbf{M}^{-1}\mathbf{B}$. Here $\mathbf{B}$ represents the transformation matrix between the Cartesian coordinates and the internal coordinates; $\mathbf{B}$ can be readily derived from the geometry of the H_2S molecule.

The vibrational energies of the different modes are the eigenvalues of the matrix $\mathbf{G}\times\mathbf{F}$; a comparison of these eigenvalues with the vibrational energies taken from literature allows one to check the accuracy of the performed calculations. Each eigenvector of this matrix corresponds to the motion of a normal mode in terms of internal coordinates. This leads us to the following relation between the changes of the normal coordinates and the internal coordinates:

$$\begin{pmatrix} \Delta r_1 \\ \Delta r_2 \\ \Delta \gamma r_0 \end{pmatrix} = \begin{pmatrix} 0.7061(2) & 0.004(1) & 0.707(0) \\ 0.7061(2) & 0.004(1) & -0.707(0) \\ -0.053(2) & 0.999(\ll 1) & 0(0) \end{pmatrix} \times \begin{pmatrix} \Delta Q_1 \\ \Delta Q_2 \\ \Delta Q_3 \end{pmatrix}. \quad (1)$$

Here, Q_1, Q_2, and Q_3 describe the symmetric stretching, bending, and asymmetric stretching vibrational mode, respectively, and r_0 is the H-S equilibrium distance in the ground state. The error bars for the matrix elements are given in units of last digit, and they result from using the different sets of force constants available in the literature [16–18]. Here "$\ll 1$" means an error small compared to the last digit, and "0" indicates exact values, resulting from group theory arguments. In the data analysis, only the excitation of the mode Q_1 was observed. This vibrational mode leads mainly to identical changes in the two H-S bond distances, but also to minor changes in the H-S-H bond angle. In principle, the matrix $\mathbf{G} \times \mathbf{F}$ should be different for each electronic state due to the different force constants and geometries. Different force constants, however, have only small influences on the matrix elements (see above). In addition, we found the influences of changes in the geometry to be even much smaller than the influences of changes of the force constants. These results justify the use of the same matrix $\mathbf{G} \times \mathbf{F}$ for all electronic states involved in the Auger process.

For both the PES and the AES, the PCI has to be taken into account. For this, the lines in the PES as well as the direct terms in the Kramers-Heisenberg equations, that describe the Auger spectra, can be approximated by a line shape given by Kuchiev and Sheinerman [19]; it is used in the present paper in its simplified form described by Armen *et al.* [20]. For the less important cross terms, we use the line shape given by the corresponding terms of the Kramers-Heisenberg equation by including an average energy shift to approximate the photoelectron relaxation. All line shapes were convoluted with a Gaussian with a width of 20 meV (FWHM) to simulate the resolution of the electron analyzer.

The background in the AES consists of a parabolic line and two broad Gaussian lines that describe Auger transitions to states unstable with respect to dissociation. In addition, four less intense and narrow Lorentzian lines were found in the spectra that will be discussed further below.

IV. RESULTS AND DISCUSSIONS

A. The photoelectron and Auger spectra

The PES and AES were measured for various photon energies $h\nu$ ranging from 180 to 240 eV. The spectra obtained at $h\nu$=230 eV are presented in Figs. 1 and 2, with the solid lines through the data points representing the fit results.

The PES in Fig. 1 consists of three main lines due to spin-orbit and ligand-field splitting. Each line shows a tail towards higher binding energies caused by PCI; in addition to this PCI tail, each main photoemission line exhibits a weak shoulder that is due to excitation of the stretching vibrational mode; these shoulders are marked by vertical arrows in Fig. 1. From the fit analysis it turns out that the relative intensities of the various S $2p^{-1}$ photoemission lines are rather independent of the excitation energy. The different relative peak heights that can be seen in the spectra measured at different excitation energies (see, e.g., Ref. [8]) are mainly due to the influence of PCI, which decreases with increasing photon energy.

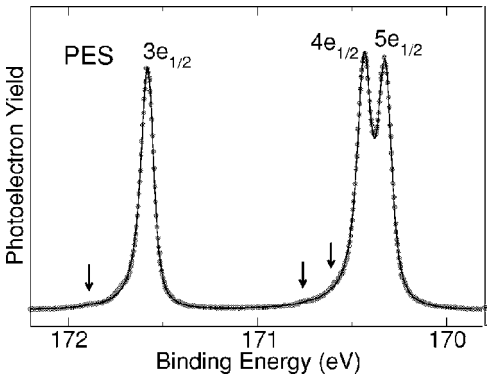

FIG. 1. The H_2S S $2p^{-1}$ photoelectron spectrum taken at a photon energy of $h\nu$=230 eV. The solid line through the data points represents the fit result. All peaks exhibit a PCI line shape accompanied by weak vibrational satellites that are indicated by vertical arrows.

In Fig. 2 a typical S $2p^{-1} \rightarrow X\ ^1A_1(2b_1^{-2})$ AES is presented. The Auger transition from the S $2p_{1/2}^{-1}$ intermediate state to the undissociative final state $2b_1^{-2}$ is shown as an example in the dashed subspectrum. Each of the transitions exhibits a rich vibrational fine structure due to large differences between the equilibrium distances of the core-excited and the final states. As in the PES, PCI influences also the line profiles of the AES, however, as a tail towards higher kinetic energies. Besides this, some additional features can be seen

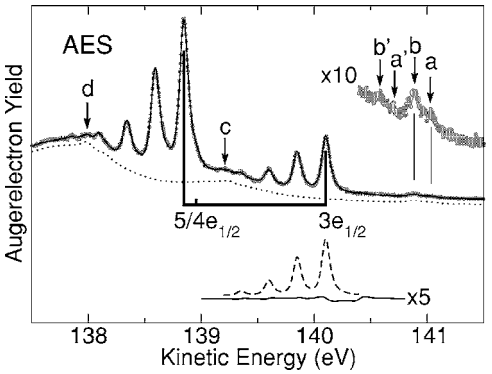

FIG. 2. S $2p^{-1} \rightarrow X\ ^1A_1(2b_1^{-2})$ Auger spectrum taken at a photon energy of 230 eV. The solid line through the data points represents the result of a fit analysis with the dotted curve representing the background. The intensities of the various S $2p^{-1} \rightarrow 2b_1^{-2}$ Auger transitions are given by the vertical-bar diagram. The dashed subspectrum, in the lower part of the figure, represents the vibrational progression of the S $2p_{1/2}^{-1}3e_{1/2} \rightarrow 2b_1^{-2}$ Auger transition, and the solid subspectrum represents the vibrational lifetime interference contributions. The vertical arrows (peaks a–d) mark weak Auger transitions that are related to multielectron excitations (see text).

TABLE I. The results of the fit analysis. Given are the changes of the equilibrium value of Q_1, ΔQ_1 relative to the ground state (g.s.), the vibrational energies $\hbar\omega_1$, the anharmonicities $x\hbar\omega_1$, the H-S bond distances r, and the H-S-H bond angles γ. The values for the intermediate state S $2p^{-1}$ and the final state $X\,^1A_1(2b_1^{-2})$ are derived from the fit analysis, and the values for the ground state are taken from the literature [14]. The values for ΔQ_1 are given in $\text{Å}u^{1/2}$, with u representing the atomic mass unit. The errors given for r and γ result from the combined errors, derived for ΔQ_1 and the matrix given in Eq. (1). Note, that the values for γ are based only on the observation of the observed stretching mode Q_1. For comparison, the vibrational energy and anharmonicity from Ref. [25] are also given.

State	g.s.	S $2p^{-1}$	$X\,^1A_1(2b_1^{-2})$	Ref. [25]
ΔQ_1 ($\text{Å}u^{1/2}$)		0.011(1)	0.139(2)	
$\hbar\omega_1$ (meV)	324.17	329(6)	258(1)	268(1)
$x\hbar\omega_1$ (meV)	8.05		2.1(0.3)	4.7(1.2)
r (Å)	1.328	1.320(1)	1.424(2)	
γ (°)	92.2	92.225(3)	91.91(1)	

in the spectra; they are marked by vertical arrows and are probably related to the Auger decay of intermediate states with multielectron excitation (see below).

From the PES and AES, a splitting between the S $2p_{3/2}^{-1}5e_{1/2}$ state and the $2p_{3/2}^{-1}4e_{1/2}$ state ($2p_{1/2}^{-1}3e_{1/2}$ state) of 111 ± 1 meV (1255 ± 1 meV), respectively, is derived. These two splittings are caused by spin-orbit and ligand-field interaction and agree well with previous experimental results given in Refs. [8,21]. The value of 90 meV for the ligand-field splitting obtained by Bueno *et al.* [9] appears too small, indicating that in that work the contributions of the S $2p_{3/2}^{-1}4e_{1/2}\rightarrow X\,^1A_1(2b_1^{-2})$ Auger transition to the spectrum were described with less accuracy. The ligand-field splitting of the S $2p_{3/2}$ state obtained in the present work agrees well with the theoretical results of Bøvre [22] of 108 meV and of Bueno *et al.* [9] of 114 meV.

For the detailed analysis of the vibrational structures only the excitation of the symmetric stretching vibrational mode was taken into account. Nevertheless, good agreement between the measurements and the fit results was obtained. Possible excitations of the bending and the asymmetric stretching vibrational modes show no contributions to the spectra, which however, is not an unexpected result. Since the electron density distribution of the final state $2b_1^{-2}$ is essentially symmetric, an excitation of the asymmetric stretching vibrational mode is not expected. The bending vibrational mode is also not noticeably excited since the main changes in intermolecular parameters occur in the H-S bondlength, but not in the bonding angle.

Table I summarizes the parameters obtained for the potential energy curves of the intermediate and the final states. Relative changes in the equilibrium values for the normal coordinate Q_1, the vibrational energies $\hbar\omega$, and the anharmonicities $x\hbar\omega$, were taken from the fit. The equilibrium geometries of H_2S in the intermediate and the final state were derived from the fit results and the geometry of the ground state [15]. The anharmonicity of the intermediate state could not be derived due to the weak vibrational progression. Both the intensities and the energy positions of the vibrational substates in the Auger transitions are described well by using the same values for $\hbar\omega$ and $x\hbar\omega$. This result makes the presence of a possible Fermi resonance between the stretching vibrational mode and the bending vibrational mode quite unlikely; such a Fermi resonance between different vibrational modes has been found for the C $1s^{-1}$ photoionization spectrum in methane and resulted in inconsistent values for the vibrational energies and anharmonicities by fitting these parameters to the intensities or the energy positions of the vibrational substates [23,24]. For comparison, the vibrational energy $\hbar\omega$ and anharmonicity $x\hbar\omega$ obtained by Eland in the direct double photoionization process are also given [25] revealing that the present values do not agree within the previous results within the limits of error.

The value and sign of ΔQ_1 between the intermediate and the final state can be taken directly from the intensity distribution of the Auger lines and the fact that the vibrational energy in the intermediate state is much higher than in the final state. It is, however, almost impossible to derive the sign of ΔQ_1 between the ground state and the intermediate state from the PES alone, since the vibrational progression in the intermediate state is so weak. As an alternative, the sign can be obtained from lifetime interference contributions in the AES.

The solid subspectra in Fig. 2 represent contributions from vibrational lifetime interference, which are significant for the high-energy side of each vibrational band. These vibrational lifetime interference terms are less intense than the direct terms, but they are sensitive to the sign of ΔQ in the excitation process.

This sign sensitivity of the vibrational lifetime interference is due to the fact that the Franck-Condon factors contribute in a linear way to the corresponding term in the Kramers-Heisenberg equation, i.e., $\langle\nu_f|\nu_i\rangle\langle\nu_i|\nu_g\rangle\langle\nu_g|\nu_i'\rangle\langle\nu_i'|\nu_f\rangle$, with ν_g (ν_f) being the vibrational wave function in the ground state (final state). ν_i and ν_i' indicate different vibrational levels in the intermediate state. The strongest vibrational lifetime interference contributions originate from a transition from $\nu_g=0$ to $\nu_f=0$ via the intermediate levels $\nu_i=0$ and 1. The sign dependence of these contributions can be explained by the symmetry of the wave functions. The wave functions $\nu=0$ are symmetric with respect to the equilibrium geometry, and the wave functions $\nu=1$ are antisymmetric; as a result, the sign of the matrix element $\langle\nu_g=0|\nu_i=1\rangle$ depends on the sign of the change in Q_i. This matrix element contributes linearly to the vibrational lifetime interference term. In the given case, the vibrational energy of the final state is much smaller than that of the intermediate state, and we have to conclude that the equilibrium distance is larger in the final state. As a result, the signs of all other matrix elements are known besides their phases, which originate from arbitrary phase factors in the vibrational wave functions. These phases, however, do not contribute to the total sign of the vibrational lifetime interference term since each wave function contributes one time as a bra vector and one time as a ket vector.

Although the vibrational lifetime interference contributions are small due to the weak excitations of higher vibra-

tional substates in the intermediate state, it is possible to determine the H-S bondlength in the S $2p$ core-ionized states as 1.320 ± 0.001 Å using these terms. This result corresponds to a change in the H-S equilibrium distance by $\Delta r = -8$ mÅ and can be compared with changes in the equilibrium distances, caused by a $2p^{-1}$ ionization of other H-containing molecules formed by the third-row elements X=Si,P,Cl. For SiH_4, a change in the Si-H equilibrium distance of $\Delta r = -55$ mÅ [26], for PH_3 a change in the P-H equilibrium distance of $\Delta r = -42$ mÅ, and for HCl a change in the Cl-H equilibrium distance of $\Delta r = +15$ mÅ [3] has been found; the value for PH_3 has been derived from the FCFs reported in Ref. [27]. Obviously, Δr increases with the atomic number of the central atom X and decreases with the number of H atoms. We relate these findings with the change of the bonding character, which is polar in case of HCl and covalent in case of SiH_4.

Electronic lifetime interference has to be taken into account if the energy splitting between two different electronic intermediate states is of the same order of magnitude as the natural linewidth. This is fulfilled in the present case only for the core holes $2p_{3/2}^{-1}4e_{1/2}$ and $2p_{3/2}^{-1}5e_{1/2}$. In the fit analysis, the electronic lifetime interference terms are described by $\alpha D_4 D_5 Q_4 Q_5$, with D_4 (D_5) being the dipole matrix element between the ground state and the $2p_{3/2}^{-1}4e_{1/2}$ ($2p_{3/2}^{-1}5e_{1/2}$) core-hole state and Q_4 (Q_5) being the Coulomb matrix element of the $2p_{3/2}^{-1}4e_{1/2}$ ($2p_{3/2}^{-1}4e_{1/2}$) Auger transition to the $2b_1^{-2}$ final state. The matrix elements $D_{4,5}$ ($Q_{4,5}$) are represented by the positive square root of the intensity of the respective photoelectron (Auger) line. The function of the additional fit parameter α is discussed in more detail in Ref. [3], while the main ideas will be repeated here. From the fit analysis, no information on the signs of the dipole and the Coulomb matrix elements can be obtained leading to the fact that $-1 < \alpha < 1$. $|\alpha| = 1$ stands for full interference, which is given if one final state is populated via two or more intermediate states that decay all only to a given final state. In the case of a normal AES, however, the intermediate states decay into different final states. In addition, a number of experimentally indistinguishable final states exist in the spectrum, since for the final states the symmetry of the photoelectron and the Auger electron have to be taken into account. Consequently, $|\alpha|$ is expected to be smaller than 1.

For a more quantitative analysis, we consider the matrix elements in the $\Lambda\Sigma$-coupling scheme. In this coupling scheme the three different core holes $3e_{1/2}$, $4e_{1/2}$, and $4e_{1/2}$ have to be described by linear combinations of the $\Lambda\Sigma$ core-hole states $1b_1^{-1}$ ($2p_x^{-1}$), $1b_2^{-1}$ ($2p_y^{-1}$), and $3a_1^{-1}$ ($2p_z^{-1}$), however, with strong mixing coefficients due to spin-orbit interaction. The ground state has A_1 symmetry and the different components of the dipole operator have a_1, b_1, and b_2 symmetry, so that the intermediate core-hole state $|n\rangle = |\lambda \epsilon' \lambda'\rangle$ is of A_1, B_1, or B_2 symmetry. Here, λ describes the core holes $1b_1^{-1}$, $1b_2^{-1}$, and $3a_1^{-1}$, while λ' stands for the symmetry of the photoelectron. This leads to nine different intermediate states and nine different final states $|f\rangle = |2b_1^{-2}(A_1)\epsilon' \lambda' \epsilon'' \lambda''\rangle$, with λ'' describing the Auger electron. Since the Coulomb matrix elements $\langle 1b_1^{-1}\epsilon' \lambda' | \frac{1}{r} | 2b_1^{-2}(A_1)\epsilon' \lambda' \epsilon'' \lambda''\rangle$ are much larger than the Coulomb matrix elements $\langle 1b_2^{-1}\epsilon' \lambda' | \frac{1}{r} | 2b_1^{-2}(A_1)\epsilon' \lambda' \epsilon'' \lambda''\rangle$ and $\langle 3a_1^{-1}\epsilon' \lambda' | \frac{1}{r} | 2b_1^{-2}(A_1)\epsilon' \lambda' \epsilon'' \lambda''\rangle$ [9], only the core hole $1b_1^{-1}$ has to be taken into account for further considerations and, as a consequence, only the three different final states $|2b_1^{-2}(A_1)\epsilon' b_1' \epsilon'' b_1''\rangle$, $|2b_1^{-2}(A_1)\epsilon' a_1' \epsilon'' b_1''\rangle$, and $|2b_1^{-2}(A_1)\epsilon' a_2' \epsilon'' b_1''\rangle$ are substantially populated. The intensities of the Auger lines derived from the spectrum are given by the sum of these three Auger transitions that cannot be distinguished in the experiment. This prevents the determination of the Coulomb matrix element for each final state individually and requires the introduction of α.

As mentioned above, electronic lifetime interference has to be taken into account only for the intermediate states $4e_{1/2}$ and $5e_{1/2}$ due to the small energy splitting. However, the core hole $5e_{1/2}$ can be described mainly by a $1b_1^{-1}$ core hole, while the core hole $4e_{1/2}$ contain only minor $1b_1^{-1}$ contributions [9]. These strong differences in the $1b_1^{-1}$ contributions to the core holes lead to only a small uncertainty about the way a given final state is populated and, consequently, to small electronic lifetime interference contributions. On the basis of the described considerations, we estimate $|\alpha| \cong \sqrt{c_1 c_2} \cong 0.096$, in good agreement with the results of the fit analysis. Here, $c_1 = 0.013$ ($c_2 = 0.709$) is the $1b_1^{-1}$ core-hole density, i.e., the square of the $1b_1^{-1}$ mixing coefficient of the $4e_{1/2}$ ($5e_{1/2}$) intermediate core-hole state [9].

As can be seen from the vertical-bar diagram in Fig. 2, the intensities of the Auger transitions, starting from the three ligand-field components, are quite different; this is in contrast to the photoelectron intensities that are quite similar for all three core holes. In particular, it is seen that the Auger transition starting from the $4e_{1/2}$ intermediate state is rather weak. The strong suppression of this Auger transition is discussed in detail in Ref. [9]. In short, the intensities of the Auger transitions are given by the spatial overlap between the intermediate and the final state. Since the different S $2p^{-1}$ core holes exhibit individual spatial orientations, this results in vastly different overlaps with the $2b_1$ orbital explaining the observed variations in the intensities.

The vibrational fine structure of the S $2p^{-1} \rightarrow 2b_1^{-2}$ Auger transition is similar to the progression in the double ionization spectrum reported by Eland [25], which leads to the same final state. This similarity of the vibrational progression is due to the small change in the equilibrium geometry upon core ionization, which is reflected by very small contributions of vibrational substates to the PES spectrum displayed in Fig. 1. In order to perform a more detailed comparison of these two vibrational progressions, we simulated the Franck-Condon envelope of a direct transition between the ground state and the $2b_1^{-2}$ final state. By using the potential energy surface of the ground state from literature and the one of the $2b_1^{-2}$ final state as obtained in the present study, we obtained an intensity ratio of 100:59(2):19(1):4(1) for the transitions $\nu' = 0 \rightarrow \nu'' = 0 : \nu'' = 1 : \nu'' = 2 : \nu'' = 3$. The error bars are based on the uncertainty in the equilibrium geometry for the $2b_1^{-2}$ final state presented in Table I. These values differ clearly from the intensity ratio of 100:50:20:6 reported by Eland [25] for the direct double photoionization by using the time-of-flight photoelectron-photoelectron coincidence method, and they show that the results of the latter technique do not

TABLE II. Relative intensities of the various Auger transitions I normalized to the S $2p_{3/2}^{-1}5e_{1/2} \rightarrow X\,^1A_1(2b_1^{-2})$ transition, and linewidths Γ for the different S $2p^{-1}$ core holes. Given are the results of the present fit analysis as well as the experimental and theoretical results of Ref. [9].

Core hole	$3e_{1/2}^{-1}$	$4e_{1/2}^{-1}$	$5e_{1/2}^{-1}$
I_{ex} [this work]	0.35±0.05	0.04±0.01	1
I_{ex} [9]	0.42±0.03	0.09±0.03	1
I_{th} [9]	0.42	0.06	1
Γ_{ex} (meV) [this work]	63±1	65±5	75±1
Γ_{ex} (meV) [9]	64±2		74±2
Γ_{th} (meV) [9]	68	59	83

follow exactly a Franck-Condon envelope as indicated already in the literature [25,28,29].

The relative intensities of the various Auger transitions are presented in Table II, together with previous experimental and theoretical results from Ref. [9]. Note that the error bars given in the present work are not based on statistical errors, but were derived from fit results of spectra taken at different photon energies and fitted with different strategies. The relative intensities obtained in the present work agree reasonably well within the limit of errors with the experimental results of Ref. [9]. The somewhat smaller values for the intensities of the S $2p^{-1}3e_{1/2} \rightarrow X\,^1A_1 2b_1^{-2}$ and S $2p^{-1}3e_{1/2} \rightarrow X\,^1A_1 2b_1^{-2}$ transitions might be due to the fact that in the present analysis lifetime interference contributions were taken into account. This can also be due to the fact that in the fit analysis of Ref. [9] a somewhat too small value for the ligand-field splitting was used (see above). The agreement with the theoretical results in Ref. [9] is also satisfactory.

The linewidths of the various S $2p^{-1}$ core holes are also given in Table II: for the S $2p^{-1}3e_{1/2}$ and S $2p^{-1}5e_{1/2}$ core holes they agree very well with the experimental results of Bueno *et al.* [9]. In contrast to Ref. [9], we could also derive the linewidth of the S $2p^{-1}4e_{1/2}$ core hole, however, with a larger error bar than for the other two core holes. This value, however, despite its large error bar, does not seem to support the theoretical prediction that the linewidth of this core hole is considerably narrower than those of the S $2p^{-1}3e_{1/2}$ and S $2p^{-1}5e_{1/2}$ core holes.

B. Decay of doubly excited states, shake-up and shake-off states, and dissociation products

In addition to the lines that are unambiguously related to the S $2p^{-1} \rightarrow 2b_1^{-2}$ normal Auger transitions of H_2S, some additional narrow lines are present in the spectra. These are indicated by vertical arrows in Fig. 2. From the relatively narrow linewidths of these weak features, it can be concluded that they originate from the decay of atomic or ionic sulphur or due to nondissociative decay into H_2S or HS; the radical HS can be formed by the dissociation of double-excitation states close to the S $2p$ ionization threshold as well as of S $2p$ core-ionized states in combination with

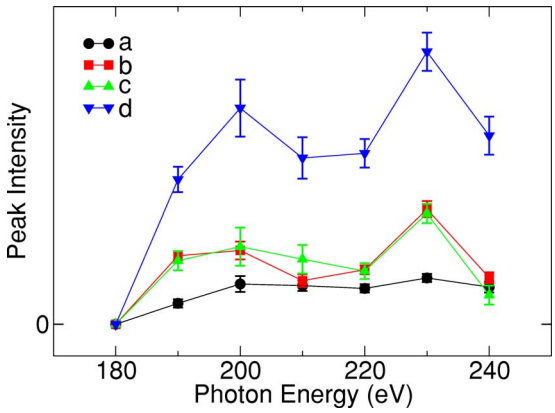

FIG. 3. (Color online) Photon energy dependence of the intensities of peaks (a)–(d) in the Auger spectra, normalized to the intensity of $3e_{1/2} \rightarrow 2b_1^{-2}$ Auger transition measured at the respective photon energy.

shake-up and shake-off satellites. An Auger decay of neutral core-excited HS^* can be excluded since those transitions would lead to higher kinetic energies for the Auger electrons [30,31]. The Auger spectra of HS^*, however, exhibit very little vibrational structure, i.e., single holes in the $3p\pi$ shell lead only to a minor weakening of the bond. Based on this observation, it is reasonable to assume that even two holes in the $3p\pi$ shell, when formed as the result of the Auger decay of core-excited HS^+, are still stable with respect to dissociation.

The peaks (a) and (b) in Fig. 2 exhibit a splitting of 140 meV that agrees within the limits of error with the ligand-field splittings of HS [31] and H_2S. In addition, at $h\nu$=230 eV, peak (b) reaches its strongest intensity, and reveals some additional weaker satellites appearing at ≅300 meV and ≅600 meV lower energies; these additional satellites can be interpreted as vibrational excitations of peak (b). All these findings suggest a molecular decay to a nondissociative final state, e.g. by a nondissociative decay of $2p$-excited HS^+, as discussed above. As an alternative assignment of peak (a) and (b), we suggest an Auger decay of a shake-up satellite of the S $2p^{-1}$ photoelectron line. This Auger decay, however, must lead to a nondissociative final state, i.e., a state with both holes in the $2b_1$ shell. Such a final state can be created via a S $2p^{-1}2b_1^{-1}n^1$ intermediate state followed by a participator Auger decay. It can be assumed that n is a Rydberg orbital, since the occupation of a $6a_1$or a $3b_2$ orbital would lead to a S $2p^{-1}6a_1$ or a S $2p^{-1}3b_2$ excitation and hence to dissociation, although no additional hole in the $2b_1$ orbital is created [31,32].

Figure 3 displays the intensities of these weak lines as a function of photon energy, normalized to the intensity of the S $2p_{1/2}^{-1} \rightarrow 2b_1^{-2}$ Auger transition. It can be seen that the intensities of peak (a) and in particular of peak (b) exhibit a resonant behavior, with one maximum at $h\nu$≅200 eV and another one at $h\nu$≅230 eV, i.e. below the S $2s$ ionization threshold. This observation, however, does not exclude an explanation with an Auger decay of a S $2p^{-1}2b_1^{-1}n^1$ resonance. The maximum at ≅200 eV agrees well with a broad structure in the photoabsorption spectrum [33] of H_2S and might be caused by direct excitation of the S $2p^{-1}2b_1^{-1}n^1$

intermediate states. The resonance at $h\nu \cong 230$ eV can be readily explained by an enhanced production of the S $2p^{-1}2b_1^{-1}n^1$ states due to excitation of S $2s^{-1}n^1$ resonances and the subsequent Koster-Kronig decay to these states [34].

Peaks (c) and (d) are found at lower kinetic energies as compared to the Auger lines of H_2S or HS. They cannot originate from the Auger decay of nondissociative H_2S or HS. We suggest, therefore, that these lines are caused by Auger decays of atomic or ionic sulphur, that is a product of the dissociation of H_2S upon creation of a core hole.

V. CONCLUSIONS

In the present work, we present the results of a detailed study of the S $2p^{-1} \rightarrow X\ ^1A_1(2b_1^{-2})$ normal Auger spectrum of H_2S. To this purpose, the S $2p^{-1}$ core-hole photoelectron spectrum and the S $2p^{-1} \rightarrow X\ ^1A_1(2b_1^{-2})$ normal Auger transitions were recorded for photon energies in the range from 180 to 240 eV. The measured spectra were fitted simultaneously with a model that includes spin-orbit and ligand-field splittings, post-collision interaction, vibrational fine structures in the core-excited and the final states, as well as vibrational and electronic lifetime interferences. This elaborate fit analysis resulted in an excellent description of the spectra and allowed us to derive detailed information about the potential energy surfaces in the core-hole and final states, i.e., the equilibrium distances r, equilibrium angles α, vibrational energies $\hbar\omega$, and anharmonicities $x\hbar\omega$. The relative intensities of the various S $2p^{-1} \rightarrow X\ ^1A_1(2b_1^{-2})$ normal Auger transitions as well as the linewidths of the different S $2p^{-1}$ core-ionized states were also obtained. The vibrational lifetime interference contributions were utilized to determine the equilibrium geometry of the core-ionized state, while the electronic lifetime interference contributions turned out to be of minor importance.

In addition to the S $2p^{-1} \rightarrow X\ ^1A_1(2b_1^{-2})$ transitions, we observed some weak lines in the Auger spectra that exhibit strong photon-energy dependences of their intensities. These lines were assigned to decay processes of multielectron excitations or dissociation products of H_2S subsequent to the excitation or ionization processes.

ACKNOWLEDGMENTS

The work at the Freie Universität Berlin was supported by the BMBF, Project No. 05 KS1 KED/0, and the Deutsche Forschungsgemeinschaft, Project No. PU 180/2. We are grateful for funding to the Research Council for Natural Sciences of the Academy of Finland and the Väisälä Foundation. The authors gratefully acknowledge the assistance of the MAX Laboratory staff during the measurements. R.P. thanks Dr. Reinhold Fink for valuable discussions.

[1] L. Karlsson, P. Baltzer, S. Svensson, and B. Wannberg, Phys. Rev. Lett. **60**, 2473 (1988).
[2] S. Svensson, L. Karlsson, P. Baltzer, M. P. Keane, and B. Wannberg, Phys. Rev. A **40**, 4369 (1989).
[3] R. Püttner, V. Pennanen, T. Matila, A. Kivimäki, M. Jurvansuu, H. Aksela, and S. Aksela, Phys. Rev. A **65**, 042505 (2002).
[4] W. Wannberg, S. Svenson, M. P. Keane, L. Karlsson, and P. Baltzer, Chem. Phys. **133**, 281 (1989).
[5] R. Püttner, Y. F. Hu, G. M. Bancroft, H. Aksela, E. Nõmmiste, J. Karvonen, A. Kivimäki, and S. Aksela, Phys. Rev. A **59**, 4438 (1999).
[6] L. Karlsson, S. Svensson, P. Baltzer, M. Carlsson-Göthe, M. P. Keane, A. Naves de Brito, N. Correia, and B. Wannberg, J. Phys. B **22**, 3001 (1989).
[7] S. Svensson, A. Naves de Brito, M. P. Keane, N. Correia, and L. Karlsson, Phys. Rev. A **43**, 6441 (1991).
[8] S. Svensson, A. Ausmees, S. J. Osborne, G. Bray, F. Gel'mukhanov, H. Ågren, A. Naves de Brito, O.-P. Sairanen, A. Kivimäki, E. Nõmmiste, H. Aksela, and S. Aksela, Phys. Rev. Lett. **72**, 3021 (1994).
[9] A. M. Bueno, A. N. de Britto, R. F. Fink, M. Bässler, O. Björneholm, F. Burmeister, R. Feifel, C. Miron, S. L. Sorensen, H. Wang, and S. Svensson, Phys. Rev. A **67**, 022714 (2003).
[10] R. Püttner, Y. F. Hu, G. M. Bancroft, A. Kivimäki, M. Jurvansuu, H. Aksela, and S. Aksela, Phys. Rev. A **68**, 032705 (2003).
[11] N. Correia, A. Flores-Riveros, H. Ågren, K. Helenelund, L. Asplund, and U. Gelius, J. Chem. Phys. **83**, 2035 (1985).
[12] M. Halmann and I. Laulicht, J. Chem. Phys. **43**, 438 (1965).
[13] H. A. Ory, A. P. Gittelman, and J. P. Maddox, Astrophys. J. **139**, 346 (1964).
[14] G. Herzberg, *Electronic Spectra and Electronic Structure of Polyatomic Molecules* (Van Nostrand, Princeton, 1966), p. 586.
[15] N. B. Colthup, L. H. Daly, and S. E. Wiberley, *Introduction to Infrared and Raman Spectroscopy* (Academic Press, New York, 1990).
[16] G. Herzberg, *Electronic Spectra and Electronic Structure of Polyatomic Molecules* (Van Nostrand, Princeton, 1945), p. 170.
[17] J. Duchesne, Mem. Soc. Sci. Liege **1**, 427/524 463 (1946).
[18] C. R. Bailey, J. W. Thompson, and J. B. Hale, Phys. Rev. **49**, 777 (1936).
[19] M. Yu. Kuchiev and S. A. Sheinerman (unpublished); Zh. Eksp. Teor. Fiz. **90**, 1680 (1986) [Sov. Phys. JETP **63**, 986 (1986)].
[20] G. B. Armen, J. Tulkki, T. Åberg, and B. Crasemann, Phys. Rev. A **36**, 5606 (1987).
[21] M. R. F. Siggel, C. Field, L. J. Sæthre, K. J. Børve, and T. D. Thomas, J. Chem. Phys. **105**, 9035 (1996).
[22] K. J. Bøvre, Chem. Phys. Lett. **262**, 801 (1996).
[23] T. X. Carroll, N. Berrah, J. Bozek, J. Hahne, E. Kukk, L. J. Sæthre, and T. D. Thomas, Phys. Rev. A **59**, 3386 (1999).
[24] T. Karlsen and K. J. Bøvre, J. Chem. Phys. **112**, 7986 (2000).
[25] J. H. D. Eland, Chem. Phys. **294**, 171 (2003).
[26] R. Püttner, M. Domke, D. Lentz, and G. Kaindl, Phys. Rev. A

56, 1228 (1997).
[27] Z. F. Liu, G. M. Bancroft, J. N. Cutler, D. G. Sutherland, K. H. Tan, J. S. Tse, and R. G. Cavell, Phys. Rev. A **46**, 1688 (1992).
[28] M. Hochlaf, R. I. Hall, F. Penent, H. Kjeldsen, P. Lablanquie, M. Lavollée, and J. H. D. Eland, Chem. Phys. **207**, 159 (1996).
[29] F. R. Bennett, A. D. J. Critchley, G. C. King, R. J. Leroy, and I. R. McNab, Mol. Phys. **97**, 35 (1999).
[30] A. Naves de Brito, N. Correia, B. Wannberg, P. Baltzer, L. Karlsson, S. Svensson, M. Y. Adam, H. Aksela, and S. Aksela, Phys. Rev. A **46**, 6067 (1992).
[31] A. Naves de Brito, S. Svensson, S. J. Osborne, A. Ausmees, A. Kivimäki, O.-P. Sairanen, E. Nõmmiste, H. Aksela, S. Aksela, and L. J. Saethre, J. Chem. Phys. **106**, 18 (1997).
[32] H. Aksela, S. Aksela, A. Naves de Brito, G. M. Bancroft, and K. H. Tan, Phys. Rev. A **45**, 7948 (1992).
[33] E. Hudson, D. A. Shirley, M. Domke, G. Remmers, and G. Kaindl, Phys. Rev. A **49**, 161 (1994).
[34] Y. Hikosaka, P. Lablanquie, F. Penent, J. G. Lambourne, R. I. Hall, T. Aoto, and K. Ito, J. Electron Spectrosc. Relat. Phenom. **137-140**, 287 (2004).